CrossMark

J. Fluid Mech. (2016), *vol.* 789, *pp.* 259–284. © Cambridge University Press 2016
doi:10.1017/jfm.2015.680

An experimental investigation into supercavity closure mechanisms

Ashish Karn[1,2], Roger E. A. Arndt[1,3] and Jiarong Hong[1,2,†]

[1]Saint Anthony Falls Laboratory, University of Minnesota, Minneapolis, MN 55455, USA

[2]Department of Mechanical Engineering, University of Minnesota, Minneapolis, MN 55455, USA

[3]Department of Civil, Environmental and Geo-Engineering, University of Minnesota, Minneapolis, MN 55455, USA

(Received 3 November 2014; revised 10 October 2015; accepted 13 November 2015; first published online 19 January 2016)

Substantial discrepancy in the conditions for attainment of different closure modes of a ventilated supercavity has existed widely in the published literature. In this study, supercavity closure is investigated with an objective to understand the physical mechanisms determining closure formation and transition between different closure modes and to reconcile the observations from prior studies under various flow settings. The experiments are conducted in a closed-wall recirculating water tunnel to image ventilated supercavity closure using high speed and high-resolution photography and simultaneously measure pressure inside the cavity. The flow conditions are varied systematically to cover a broad range of water velocity, ventilation flow rate and cavitator size, which correspond to different Froude numbers, air entrainment coefficients and blockage ratios, respectively. In addition to the classical closure modes reported in the literature (e.g. re-entrant jet, twin vortex, quad vortex, etc.), the study has revealed a number of new closure modes that occur during the transition between classical modes, or under very specific flow conditions. Closure maps are constructed to depict the flow regimes, i.e. the range of Froude number and air entrainment coefficient, for various closure modes at different blockage ratios. From the closure map at each blockage ratio, a critical ventilation flow rate, below which the supercavity collapses into foamy cavity upon reduction of Froude number, is identified. The air entrainment coefficients corresponding to such critical ventilation rate are found to be independent of blockage ratio. It has been observed that in the process of generating a supercavity by increasing ventilation flow rate, the cavitation number gradually reduces to a minimum value and stays fixed upon further increments in the ventilation rate. Once a supercavity is formed, the ventilation rate can be decreased to a much lower value with no change in cavitation number while still maintaining a supercavity. This process is accompanied by a change in closure modes, which generally goes from twin vortex, to quad vortex, and then to re-entrant jet. In addition, the blockage effect is shown to play an important role in promoting the occurrence of twin-vortex closure modes. Subsequently, a physical framework governing the variation of different closure modes is proposed, and is used to explain mode transition upon the change of flow conditions, including the blockage effect. This framework is further extended to shed light on the occurrence of closure modes for ventilated supercavitation experiments across different types of flow facilities, the natural supercavity closure and the pulsating supercavity reported in the literature.

† Email address for correspondence: jhong@umn.edu

https://doi.org/10.1017/jfm.2015.680 Published online by Cambridge University Press

Finally, in combination with a recent numerical study, our research discusses the role of the internal flow physics on the observed features during supercavity formation and closure-mode transition, paving the way for future investigations in this direction.

Key words: bubble dynamics, cavitation, multiphase flow

1. Introduction

Supercavitation is a special case of cavitation which can be employed to create a bubble of gas inside water, large enough to encompass an object travelling through it. It greatly reduces the skin friction drag on the object, enabling achievement of high speeds under water. The creation of a supercavity is thus of great interest for naval applications, e.g. high-speed underwater vehicles. From an initially non-cavitating flow, the conditions required for a moving object underwater to form a natural supercavity are very stringent. Therefore, ventilation is generally used to form a supercavity artificially, by blowing non-condensable gas into the low-pressure region at the rear part of the moving object. Ventilated supercavitation has been investigated by many prior researchers through analytical, experimental and numerical approaches. This process generally depends on the physical parameters such as incoming velocity (U), ventilation flow rate ($\dot{Q}_A$), ambient pressure (P_∞), cavity pressure (P_C) and cavitator diameter (d_C). These parameters are commonly expressed using following dimensionless groups: Froude number, $Fr = U/\sqrt{gd_C}$; air entrainment coefficient, $C_Q = \dot{Q}_A/Ud_C^2$; cavitation number, $\sigma_C = (P_\infty - P_C)/(1/2\rho U^2)$ etc., where g and ρ denote gravitational acceleration and water density, respectively. The prior studies in the area of ventilated supercavitation focus on deriving empirical or semi-empirical relations for these dimensionless quantities to characterize supercavity geometry and ventilation demand, which is the amount of gas required to form and sustain a supercavity (Epshtein 1973; Logvinovich 1973; Spurk & König 2002). It has been shown that the ventilation demand depends not only on the flow conditions, but also on specific features of the flow patterns in the cavity sealing zone, commonly referred to as the closure mechanism or closure mode (Logvinovich 1973). Although a variety of supercavity closure modes have been identified and studied separately, there is no universally accepted theory on the relationship between closure mechanism and ventilation demand as yet (Semenenko 2001*a*). To accurately estimate gas requirements for underwater applications using supercavitation, it would be profitable to systematically study the closure mechanisms under different flow conditions and determine the criteria that govern the transition among different closure modes.

To date, many authors have studied different closure modes, and the empirical relationships governing different closure modes have been discussed (e.g. Cox & Clayden 1956; Campbell & Hilborne 1958; Kapankin & Gusev 1984; Semenenko 2001*a*; Kawakami & Arndt 2011). In the published literature on ventilated supercavitation, four main closure modes have been widely reported: re-entrant jet (RJ), twin vortex (TV), quad vortex (QV) and pulsating cavity (PC). The RJ closure is reported to occur when Fr is high, i.e. when the effect of gravity is not significant. In such a case, the hydrostatic pressure gradient is negligible as compared to the dynamic forces and thus the cavity closely resembles an axisymmetric shape. The cavity rear end fills with foam which is periodically ejected in the form of toroidal vortices (Semenenko 2001*a*). The TV closure is usually observed at low Fr and

https://doi.org/10.1017/jfm.2015.680 Published online by Cambridge University Press

σ_c values, when the effect of gravity becomes predominant. According to Cox & Clayden (1956), for TV closure, the locus of the centroids of the cavity section tends to rise under buoyancy forces, and the cavity is effectively cambered upwards and is no longer axisymmetric. The circulation set-up around the supercavity due to the hydrostatic pressure gradient produces a lift force which is equal and opposite to the buoyancy force on the bubble. This circulation about the cavity mid-plane, associated with this lift force, sheds downstream in the form of two counter-rotating vortices. Thus, this streamwise vorticity due to the cavity asymmetry eventually splits the supercavity lengthwise into two vortex tubes through which the ventilation air escapes out of the supercavity. Although a significant number of studies have been conducted to investigate the criteria for the formation of TV and RJ closure and their transitions (e.g. Campbell & Hilborne 1958; Buyvol 1980; Spurk & König 2002), there is a lack of agreement on the empirical formulations and physical phenomena reported from different studies (e.g. Peng *et al.* 2006; Zhang *et al.* 2007; Zhou *et al.* 2010; Kawakami & Arndt 2011; Skidmore *et al.* 2015). For instance, the first such empirical criterion for transition was given by Campbell & Hilborne (1958) based on experiments conducted in a whirling arm channel for a limited range of Fr from 5 to 25. Their experiments show that a RJ cavity occurs at $\sigma_C Fr > 1$, and a TV cavity forms at $\sigma_C Fr < 1$. Later, Buyvol (1980) proposed the criterion for the existence of a RJ cavity as $\sigma_C^{1.5} Fr^2 > 1.5$. More recently, a slightly different condition for a RJ cavity is provided by Spurk & König (2002) as $\sigma_C Fr^2 > 1$. However, contrary to the published reports, experiments at Saint Anthony Falls Laboratory (SAFL) show that the RJ closure occurs at low Fr, and is not observed even at very high values of $\sigma_C Fr$ (Kawakami & Arndt 2011). Similar to Kawakami & Arndt (2011), many other studies reported only one closure mode across a wide range of σ_C and Fr, and found other types of closures to be conspicuously unattainable. For example, some studies have only reported the occurrence of a TV closure in their closed-wall water tunnel (e.g. Cox & Clayden 1956; Kawakami 2010; Zhou *et al.* 2010) or free-surface channel (e.g. Campbell & Hilborne 1958), while others only observe a RJ closure in a closed-wall water tunnel facility (e.g. Gadd & Grant 1965; Skidmore 2013). The QV mode is a special case of a stable vortex closure, where each vortex of the TV further splits into two such that one pair of vortices lies above the other. The QV was first reported by Kapankin & Gusev (1984), and more recently by Kawakami & Arndt (2011) at low Fr and C_Q values. However, the formation mechanism and criterion for this closure are not well understood. The PC closure, first observed by Silberman & Song (1961), has been reported in many other studies (e.g. Song 1961; Karlikov *et al.* 1987; Semenenko 2001*a*,*b*; Skidmore 2013), typically at high air entrainment rates. This regime is different from other closure types since the entire supercavity has a wavy surface, and the gas loss is primarily due to periodic ejections of an air–water mixture at the rear of the supercavity, causing great variation in its length. Akin to other closure modes, the conditions governing the occurrence of pulsating cavities are also not clear (Silberman & Song 1961; Michel 1984; Stinebring *et al.* 2001; Paryshev 2003).

The observed discrepancies from the above-mentioned studies in predicting the supercavity closure mode can be attributed to several factors, e.g. the nature of experimental facility (e.g. towing tank, closed-wall tunnel versus free-surface facility, etc.), blockage (defined in terms of percentage as $B = d_C/D_T$, where D_T is the tunnel equivalent diameter) etc., but the exact bearings of the variation of these parameters on supercavitation phenomena are not understood on a fundamental physical level. Hence, in this study, we have attempted an in-depth investigation into

https://doi.org/10.1017/jfm.2015.680 Published online by Cambridge University Press

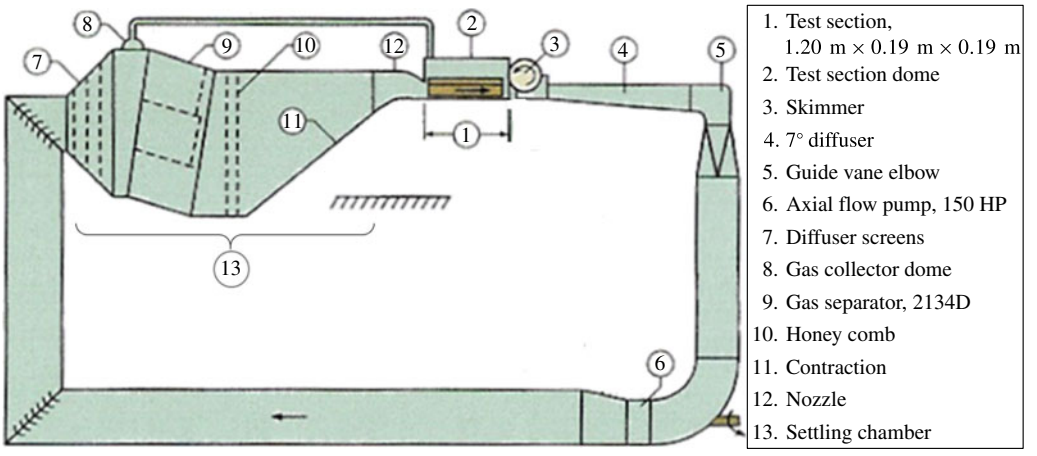


FIGURE 1. (Colour online) Schematic of the SAFL water tunnel facility.

the phenomena of supercavity closure in order to better understand the impact of flow conditions, including the blockage and the flow facility on the dynamics of ventilated supercavities.

The current paper is structured as follows: § 2 provides the details of the experimental methods. In § 3, experimental observations on supercavity closure under different flow conditions are reported. Subsequently, in § 4, we propose a theory to explain the occurrence of different supercavity closure modes observed in our experiments. The fundamentals are laid out in § 4 and are further extended to discuss the results of prior studies conducted across different experimental facilities and other characteristics of supercavitation in § 5.

2. Experimental methods

The experiments were conducted to image ventilated supercavity closure and to obtain the corresponding pressure measurements inside the cavity under different flow conditions. The study was conducted at the Saint Anthony Falls Laboratory's high-speed water tunnel, which is shown as a schematic in figure 1. It is a recirculating, closed-jet facility with absolute pressure regulation. It has a horizontal test section of 1.20 m in length, with a 0.19 m × 0.19 m square cross section (i.e. 0.21 m in hydraulic diameter). The two side walls and the bottom wall of the test section are made of Plexiglas for optical access. The tunnel is designed for cavitation and air ventilation studies and is capable of operating at a velocity in excess of 20 m s^{-1} with a turbulence level of approximately 0.3 %. As shown in figure 1, the facility includes a large dome-shaped settling chamber, which provides for fast removal of the air bubbles generated during cavitation and ventilation experiments. This feature allows the cavitation experiments to be conducted for extended periods with little change in test-section conditions.

The ventilated supercavitation experiments were performed with the backward facing cavitator model, as described in Kawakami & Arndt (2011) and shown in figure 2. In the backward facing model, a thin NACA0012 hydrofoil strut is placed upstream of the cavitator to avoid the interaction between the formed cavity and the strut body, leading to a free closure, as reported by Logvinovich (1973). To minimize the disturbance to the flow, the thickness of the hydrofoil strut is just enough to

https://doi.org/10.1017/jfm.2015.680 Published online by Cambridge University Press

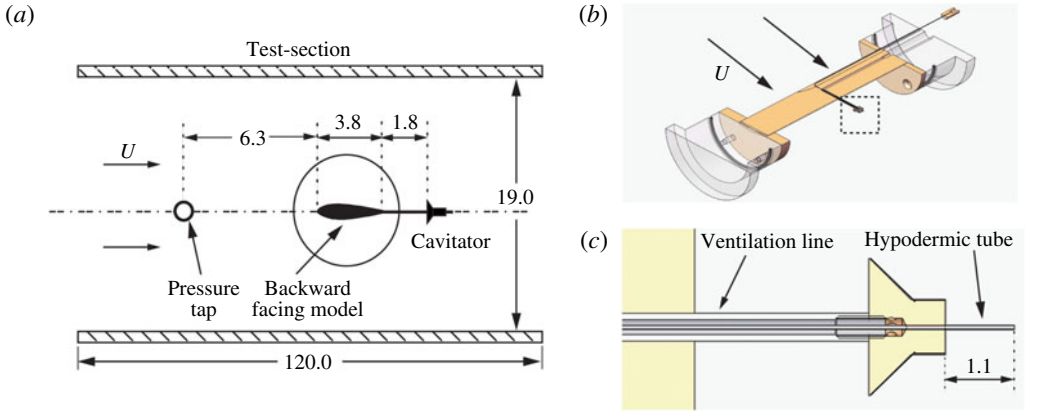


FIGURE 2. (Colour online) (*a*) A side view of the test section and the mounting configuration of the backward facing cavitator. (*b*) A sectional view and (*c*) a close-up view of the cavitator, ventilation line and the hypodermic tube used for pressure measurement. The dimensions shown in the figure are in centimetres.

envelope the ventilation pipe running to the cavitator. The maximum thickness and the chord length of the hydrofoil are 5 mm and 41 mm, respectively. The hydrofoil spans the test section and is mounted near its geometric centre. The angle of attack of the hydrofoil is measured between the axis of the test section and the axis perpendicular to the flat surface of the disk cavitator. For all the results reported in this paper, the angle of attack is fixed at 0° with a measurement uncertainty of $\pm 0.5°$. Both the cavitators and the hydrofoil are made of brass and polished to a smooth finish. High-speed videos of the supercavity under such a configuration reveal that the thin and streamlined hydrofoil strut upstream does not produce a considerable disturbance, and only a slight wake signature is observed on the side of the cavity.

The images and the videos of the supercavity closure are obtained with a $1k \times 1k$ pixel Photon APX-RS camera, which is capable of acquiring 3000 frames s^{-1} at full resolution. To ensure uniform backlighting in these videos and images, a light shaping diffuser is placed between the light source and the flow. Pressures in the test section and the supercavity are measured using two separate Validyne AP-10 pressure transducers. A Validyne DP-10 differential pressure transducer is employed to measure the differential pressure between the settling chamber and test section and is used to calculate test-section velocity. The pressure transducers are calibrated before each experiment and the pressure lines are purged with compressed air once before the pressure measurements are recorded at each condition. The calibrations are performed using a mercury manometer for both transducers. The pressure transducer calibrations are linear, with R-squared values typically 0.9999 or higher for both transducers. Standard errors of the pressure calibrations are approximately 0.1 kPa for both absolute pressure transducers. These errors lead to a maximum error of 0.11 m s^{-1} in the velocity measurement, with a mean error of approximately 0.02 m s^{-1} (Karn, Arndt & Hong 2015*a*).

The imaging of the supercavity closure and pressure measurements are conducted with four sizes of cavitators: 10, 20, 30 and 40 mm in diameter (corresponding to $B = 5\,\%$, $9\,\%$, $14\,\%$ and $19\,\%$, respectively), across a wide range of test-section flow speeds and ventilation flow rates. Test-section flow speed is controlled through the rotational velocity of the tunnel's axial flow impeller which is driven with a 75 HP

https://doi.org/10.1017/jfm.2015.680 Published online by Cambridge University Press

alternating current motor. During experiments, tunnel water temperature is monitored using a YSI thermistor, which varies between 16 and 22 °C over the course of the tests. In our experiments, the water surface in the settling chamber is vented to the atmosphere, and the test-section pressure is determined by the water velocity inside. Since the cross-sectional area of the settling chamber is significantly larger than that of the test section, the water velocity in the settling chamber is negligible compared to that in the test section. Thus, from a conservation of energy principle, as the water velocity in the test section increases, the test-section pressure decreases. The ventilation flow rate to the cavitator is controlled and measured by an Omega Engineering FMA-2609A mass flow controller. In our experiments, air flux is reported at standard conditions (i.e. a temperature of 273 K and a pressure of 1 bar) in terms of standard litres per minutes (SLPM). In the current work, the corresponding air entrainment coefficient at standard conditions is defined as $C_{Qs} = \dot{Q}_{As}/Ud_C^2$, where $\dot{Q}_{As}$ represents the air ventilation flow rate at standard conditions which is a direct reading from the mass flow controller. It is worth noting that in the present study, the mass flow rate (or volume flow rate at standard conditions) is employed instead of the volume flow rate used in the literature to give a sense of the ventilation requirement corresponding to each specific type of closure. The rationale behind adapting this definition is that, for the operation of supercavitating vehicles, it is the mass flow rate of air that determines the ventilation requirements to be carried on board. The full-scale reading of the MFC is 55 SLPM and the uncertainty in the flow measurement is $\pm 1\,\%$ of the full-scale reading. A few data points in our experiments are also collected at flow rates exceeding 55 SLPM. These large ventilation flow rates are regulated by a valve at the inlet to an Omega Engineering rotameter with a maximum mass flow rate of 100 SLPM. Factory calibrations are used for the rotameter and the uncertainty in the rotameter's scale is less than $2\,\%$ of the value. Overall, in our experiments, the maximum uncertainty in the measurement of C_{Qs}, Fr and σ_C are estimated to be $2\,\%$, $2\,\%$ and $2.2\,\%$, respectively.

3. Experimental observations

3.1. *Observations of different closure modes*

There are a variety of closure modes observed in our experiments, with the vortex-based closure mode being dominant. The acronyms and the names of different closure modes are summarized in table 1. In general, there are four stable states of a ventilated supercavity (figure 3), which include three stable closure modes (i.e. RJ, TV and QV), and the foamy cavity (FC). The FC refers to the state before the clear supercavity is formed, when the cavity consists of bubbles and foam without a clear gas–water interface (Savchenko 2001). In addition, as shown in figure 4, five unstable closure modes are discovered in our experiments, i.e., hybrid quad vortex and re-entrant jet closure (QVRJ), hybrid twin vortex and quad vortex closure (TVQV), hybrid twin vortex and re-entrant jet closure (TVRJ), a pulsating twin-vortex closure (PTV) and an interacting vortex closure (IV). These unstable modes are either observed at the transition of two stable closure modes or at high ventilation flow rates (>55 SLPM). For example, a QVRJ closure occurs at the transition of QV and RJ closure, and is characterized by a foamy end with four vortices, exhibiting the characteristics of both QV and RJ (figure 4*a*). TVQV closure is formed during the transition between QV and TV modes (figure 4*b*). The number of vortices for TVQV changes intermittently at the closure, fluctuating between one and four and with the bottom two being usually more stable than the upper ones. The TVRJ

https://doi.org/10.1017/jfm.2015.680 Published online by Cambridge University Press

Acronym	Name
RJ	Re-entrant jet closure
TV	Twin-vortex closure
QV	Quad vortex closure
FC	Foamy cavity
QVRJ	Hybrid quad vortex and re-entrant jet closure
TVQV	Hybrid twin vortex and quad vortex closure
TVRJ	Hybrid twin vortex and re-entrant jet closure
PTV	Pulsating twin-vortex closure
IV	Interacting vortex closure
PC	Pulsating cavity closure

TABLE 1. The acronyms and the names of different closure modes observed in our experiments. Note that FC listed here is considered as a state of supercavity not a closure mode. High speed videos of some of these closure modes have been provided as supplemental movies (see supplementary material available at http://dx.doi.org/10.1017/jfm.2015.680).

mode yields similar features as those of QVRJ, but only two vortices appear at the closure (figure 4*c*). At ventilation flow rates above 55 SLPM, an IV mode is observed, where the two vortices interact with each other to form one single thick vortex at the closure (figure 4*d*). At flow conditions similar to that for IV but at lower blockage (i.e., $B = 5\,\%$), PTV occurs, where both the vortices pulsate in longitudinal direction, and the cavity end intermittently breaks into elongated air pockets due to Kelvin–Helmholtz instability on the cavity surface (Kuklinski, Castano & Henoch 2001). Note that the PC reported in the literature (Silberman & Song 1961; Skidmore 2013) is not observed in our experiments, and more information including images of PC can be found in a recent paper by Skidmore *et al.* (2015).

The trends of these closure modes and the transitions between them are studied by varying the parameters Fr and C_{Qs}. A closure map is obtained (Fr versus C_{Qs}) by holding Fr constant and lowering C_{Qs} from 10 to 0.001. Figure 5 shows the closure map at a fixed blockage of $B = 5\,\%$, which corresponds to the lowest blockage in our experiments. In this closure map, a movement along the x-axis corresponds to a fixed Fr (or constant water velocity) and increasing C_{Qs}, while the slanted curves denote the lines of each fixed ventilation flow rate.

The closure map identifies separate regimes for a foamy cavity state and a supercavity state where different closure modes are observed (figure 5). In general, a foamy cavity state occurs at very low values of C_{Qs} (< 0.01), when the ventilation flow rate, dependent on Fr, is not sufficient to sustain a supercavity. In particular, a critical ventilation flow rate, Q_{crit} (defined at standard conditions) of 1.0 SLPM for the chosen cavitator (marked as a red dash-dotted line) is identified, which governs the transition from the supercavity state to the foamy cavity state. Above this critical ventilation rate, the supercavity does not transition to a foamy cavity as Fr is reduced, even to very low values. On the other hand, below this critical ventilation rate, the supercavity collapses into a foamy cavity as Fr deceases from an initial high value.

In a supercavity state, the regime for each closure mode, represented by the range of Fr and C_{Qs}, can be clearly identified in the closure map (figure 5). For stable closure modes, the TV occurs at high values of C_{Qs} and Fr ($C_{Qs} > 0.2$, $Fr > 20$), while QV is concentrated in moderate C_{Qs} and Fr ($C_{Qs} = 0.03$–0.15, $Fr = 12$–20). In comparison,

https://doi.org/10.1017/jfm.2015.680 Published online by Cambridge University Press

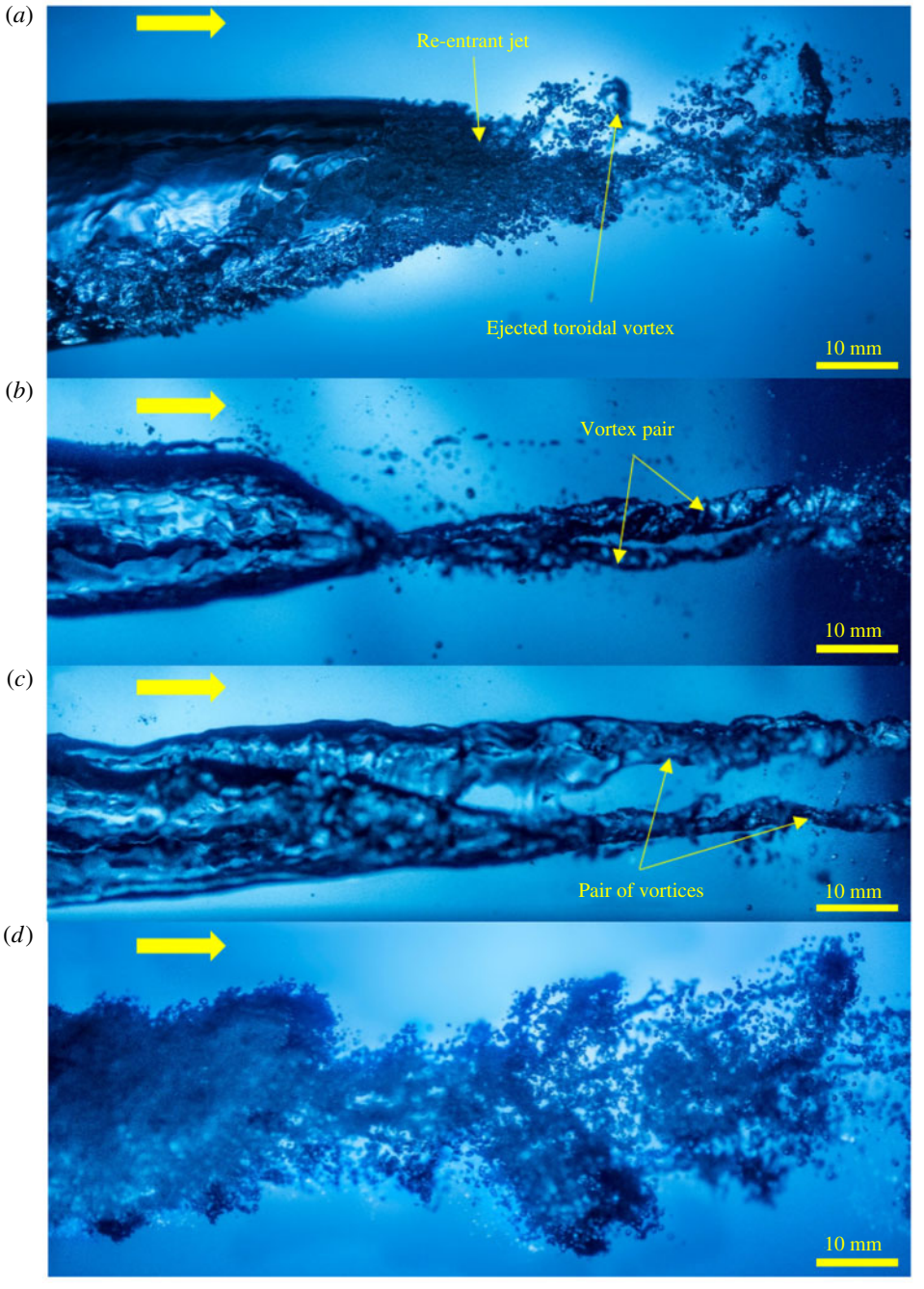


FIGURE 3. (Colour online) Side views of various stable states of the ventilated supercavity observed in our experiments: (*a*) RJ, (*b*) TV, (*c*) QV, (*d*) FC. All the images are obtained for the 20 mm cavitator, corresponding to $B = 9\,\%$. Note that the vortices are filled with air, and one vortex is hidden behind the other for both TV and QV closures due to the perspective of the camera. The horizontal arrow in the figures indicates the direction of water flow.

https://doi.org/10.1017/jfm.2015.680 Published online by Cambridge University Press

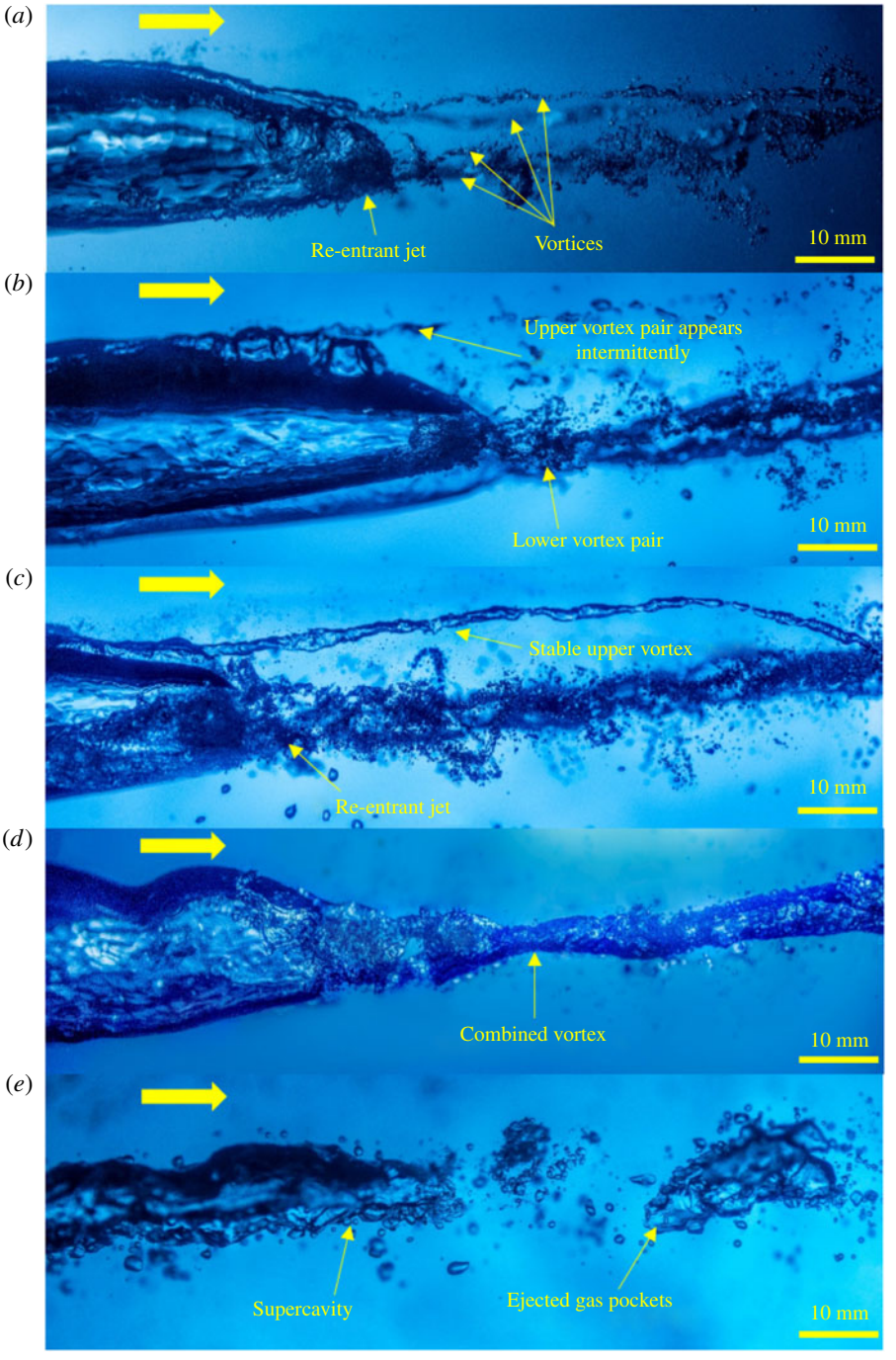


FIGURE 4. (Colour online) Side views of the various unstable closure modes observed in our experiments: (*a*) QVRJ, (*b*) TVQV, (*c*) TVRJ, (*d*) IV, (*e*) PTV. PTV mode is observed at $B = 5\,\%$ while all other modes correspond to $B = 9\,\%$. Note that the vortices are filled with air, and one vortex is hidden behind the other for both TV and QV closures due to the perspective of the camera. The horizontal arrow in the figures indicates the direction of water flow.

https://doi.org/10.1017/jfm.2015.680 Published online by Cambridge University Press

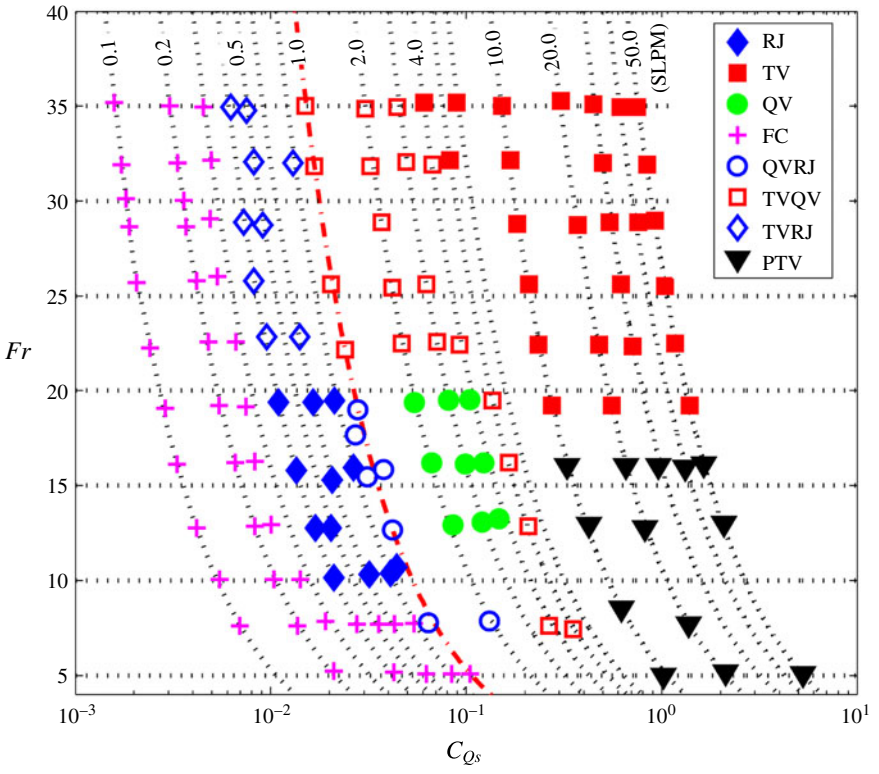


FIGURE 5. (Colour online) Closure map of different closure modes at $B = 5\,\%$. The slanted dotted lines denote lines of fixed ventilation flow rates. The values of the ventilation flow rate (in SLPM) are indicated on a selected number of the curves. The red dash-dotted line denotes the line of 'critical ventilation flow rate'.

RJ closure appears at low to moderate Fr ($Fr = 10$–20) and in a narrow range of small C_{Qs} ($= 0.02$–0.04). It has been found that RJ closure is susceptible to transition upon small changes in Fr or C_{Qs}, and a rapid reduction in C_{Qs} (at a fixed Fr) leads to supercavity collapse (a further discussion on this susceptibility is provided in § 5.4). The unstable modes are located in the transitional regimes between different stable modes. Specifically, the regimes of TVRJ and QVRJ are adjacent to the RJ regime, but situated at a higher values of Fr and C_{Qs}, respectively. Upon an increase in C_{Qs} from TVRJ, the closure mode migrates to TVQV and then to TV. Similarly, with further increment of C_Q, the supercavity transits gradually from QVRJ to QV, and TVQV. At very high C_{Qs} (> 0.5), the supercavity becomes less stable and PTV is observed. It is noteworthy that each closure mode shown in the closure map is independent of the path taken to obtain it as long as the path does not intersect with the foamy cavity state. In other words, the same closure map can be depicted by changing Fr or C_{Qs} in many other ways provided a supercavity is maintained during the variation of flow conditions.

To elucidate the interrelationships between σ_C, C_{Qs} and different cavity states, the variation in cavity states upon a change in C_{Qs} are examined at two selected Fr numbers. As figure 6 shows, at both Fr numbers, upon increment in C_{Qs}, σ_C decreases for a foamy cavity and the cavity size increases until a supercavity (i.e. the cavity

https://doi.org/10.1017/jfm.2015.680 Published online by Cambridge University Press

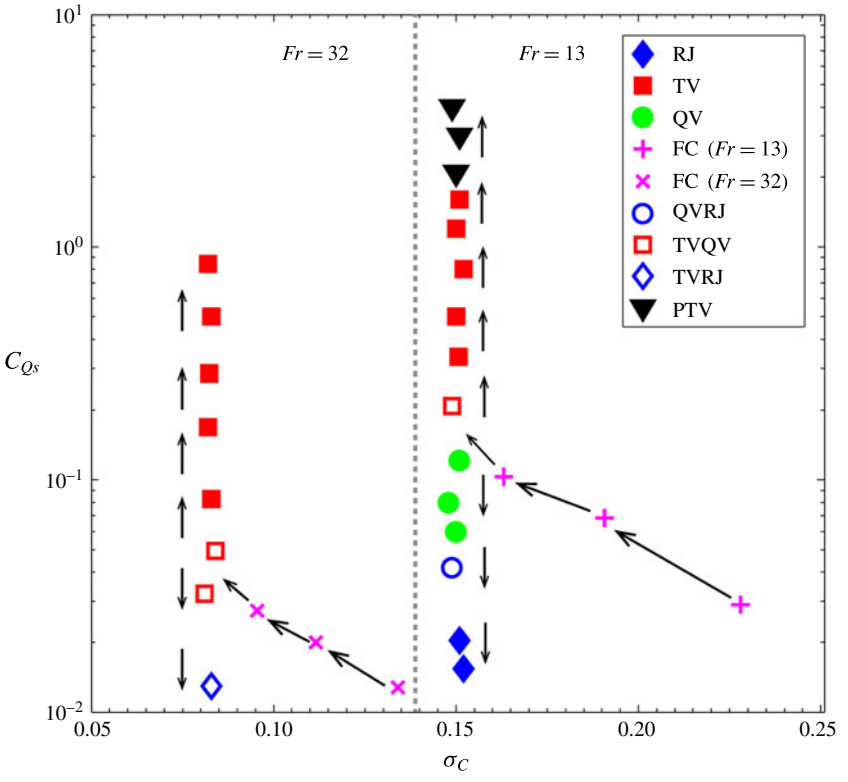


FIGURE 6. (Colour online) Variation of different closure modes upon the change of C_{Qs} for two selected Fr numbers at $B = 5\,\%$. The arrows denote gradual changes in ventilation flow rate. The dotted vertical line in the middle separates the data points corresponding to the two Fr numbers.

with a clear interface) is formed. With further increase in C_{Qs}, σ_C does not change and the supercavity yields TV closure. More interestingly, as long as a supercavity state is attained, C_{Qs} can be decreased to very low values while still maintaining the cavity and the same σ_C. This phenomenon is referred to as 'ventilation hysteresis', and has been reported by a few prior studies (e.g. Song 1961; Savchenko 2001; Kawakami & Arndt 2011). As shown by our experiments, although such a decrement in C_{Qs} does not alter σ_C, the cavity closure changes from TV to RJ. Since σ_C stays fixed and the test-section pressure does not change appreciably upon the variation in ventilation flow rate, it can be inferred that the pressure inside the supercavity does not vary with C_{Qs}. Therefore, the simultaneous change in closure mode indicates that the internal supercavity pressure is determined not only by a combination of Fr and C_{Qs}, but also the supercavity closure mechanism. This implication can be related to Spurk & König's theory (Spurk & König 2002), which suggests that the supercavity closure is associated with a change in streamline curvature at the cavity rear portion. Specifically, the curvature of the RJ mode effectively limits ventilation leakage at the closure, promoting pressure build-up inside the cavity. Thus, although the value of C_{Qs} for a RJ closure is significantly lower than that of a TV mode, the pressure inside the supercavity stays nearly the same as that of a TV mode.

https://doi.org/10.1017/jfm.2015.680 Published online by Cambridge University Press

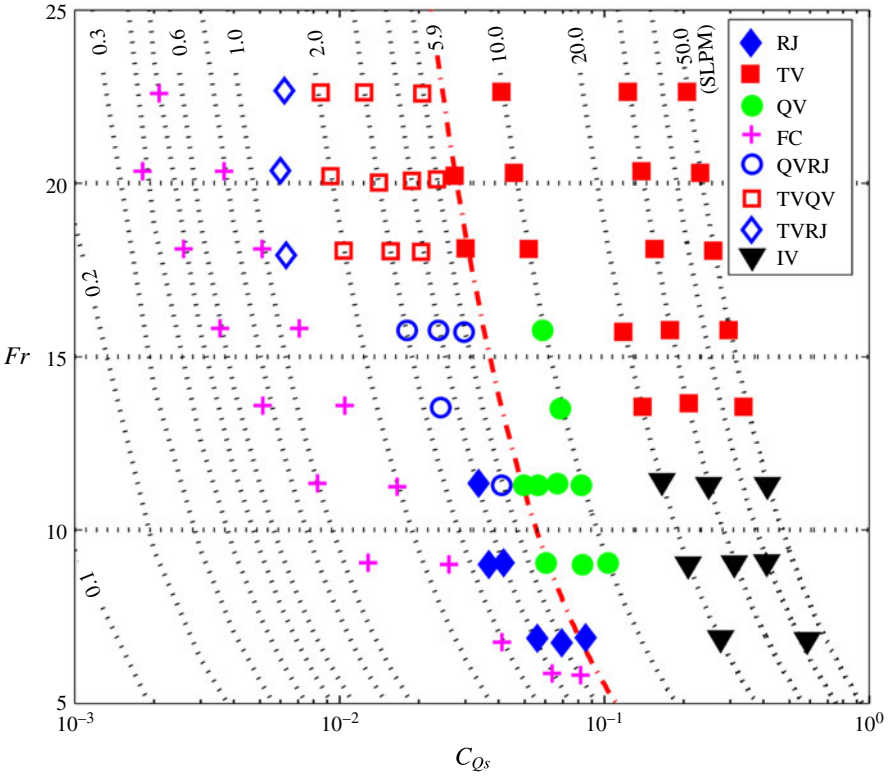


FIGURE 7. (Colour online) Closure map of different closure modes at $B = 9\,\%$. The slanted dotted lines denote lines of fixed ventilation flow rates. The values of the ventilation flow rate (in SLPM) are indicated on a selected number of the curves. The red dash-dotted line denotes the 'critical ventilation flow rate'.

3.2. *Blockage effects*

To examine the blockage effect on closure modes, figure 7 shows a closure map for $B = 9\,\%$ in comparison with the one for $B = 5\,\%$ presented in figure 5. The comparison shows that the trends for the distribution of closure modes are similar, except that the PTV closure, which appears in the bottom right of the closure map for $B = 5\,\%$, is replaced by the IV closure for $B = 9\,\%$. It is noteworthy that, essentially, both PTV and IV closures are unstable variants of the TV mode obtained at low Fr and high C_{Qs}. At higher blockages, the closure maps remain largely the same, and are thus not shown here for brevity.

According to figure 7, a critical ventilation rate has also been identified at higher blockage. This critical rate grows with increasing blockage, as shown in table 2. Moreover, an interesting aspect of the critical air entrainment becomes evident when the data are further analysed by plotting the critical air entrainment coefficient ($C_{Qs,crit}$) versus Fr (figure 8). As shown, the curves for the critical air entrainment at different blockage ratios collapse onto a single hyperbolic curve, i.e. $Fr \times C_{Qs,crit} = 0.532$, which suggests that the characteristics of the critical air entrainment is independent of the blockage effect.

As shown in figure 6, σ_C reaches a minimum value when a supercavity state is attained, and stays fixed upon further changes in C_{Qs}. Here, the trend of σ_C with

https://doi.org/10.1017/jfm.2015.680 Published online by Cambridge University Press

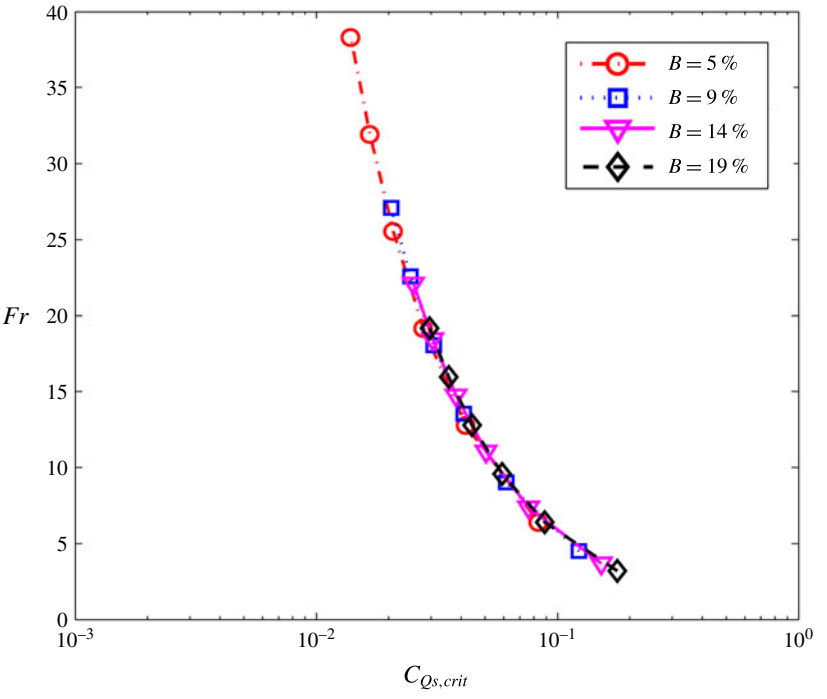


FIGURE 8. (Colour online) Relationship between Fr and $C_{Qs,crit}$ for different blockage ratios.

B (%)	Q_{crit} (SLPM)
5	1.0
9	5.9
14	16.4
19	34.0

TABLE 2. Critical ventilation flow rates at different blockage ratios.

varying Fr is examined at different blockage ratios in figure 9. For each blockage ratio, σ_C decreases at different rates as Fr increases. As high values of Fr are approached, σ_C reaches a minimum value ($\sigma_{C,min}$), and further reduction in σ_C is limited with any further increment in Fr. For $B = 5\,\%$, $9\,\%$, $14\,\%$ and $19\,\%$, the values of $\sigma_{C,min}$ are 0.08, 0.21, 0.35 and 0.51, and are obtained at Fr of 32, 18, 14 and 11, respectively. Such dependence of σ_C on Fr can be attributed to the choking phenomenon encountered in a closed-wall water tunnel due to the blockage effect (Gadd & Grant 1965; Kawakami 2010). Using control volume analysis, Kawakami (2010) showed that σ_C can be approximated by the maximum diameter of the supercavity (D_C) and the hydraulic diameter of the closed-wall water tunnel as

$$\sqrt{1+\sigma_c} = \left(1 - \left(\frac{D_C}{D_T}\right)^2\right)^{-1}. \tag{3.1}$$

https://doi.org/10.1017/jfm.2015.680 Published online by Cambridge University Press

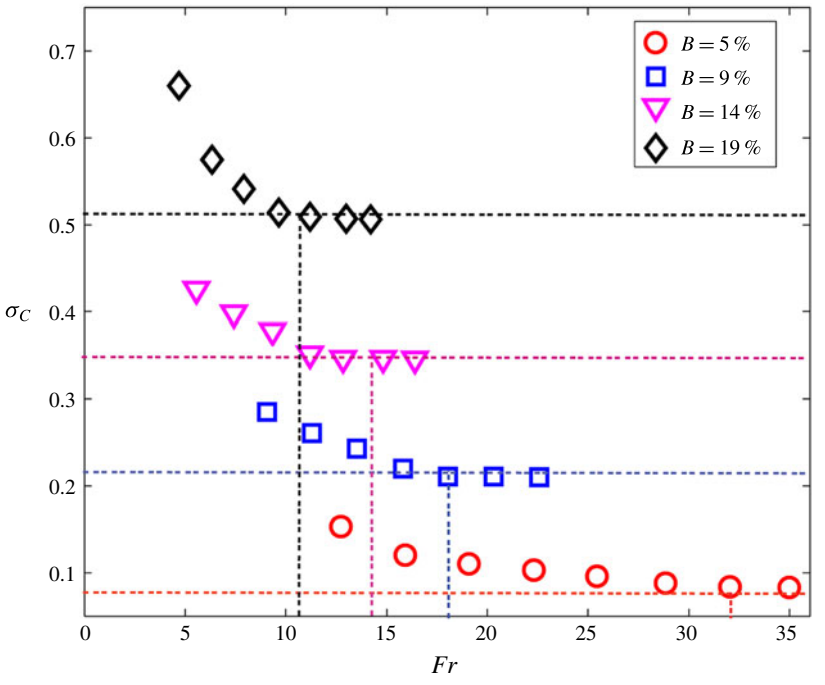


FIGURE 9. (Colour online) Variation of σ_C with Fr at different blockage ratios. The dotted lines indicate the minimum values of σ_C and the corresponding Fr when σ_C reaches minimum.

The above expression suggests a dependence of σ_C on D_C. Since our observations show that D_C depends upon Fr for a fixed blockage, and it attains a minimum with an increase in Fr, a consequent decrement in σ_C is limited with increasing Fr.

The blockage effect on the occurrence of different closure modes is further investigated under a range of flow conditions defined using 'Flow number' (F_L) according to a prior study of ventilated cavitation by Kshatriya, Patwardhan & Eaglesham (2007), and Reynolds number (Re). The F_L is a dimensionless number defined as $F_L = \dot{Q}_{As}/\dot{Q}_{Ws}$, where $\dot{Q}_{As}$ and $\dot{Q}_{Ws}$ are the air ventilation flow rate and water flow rate at standard conditions through the test section, respectively. The Re is constructed using the incoming flow velocity, hydraulic diameter of the water tunnel and kinematic viscosity (ν) according to $Re = UD_T/\nu$. Unlike C_{Qs} and Fr, F_L and Re offer a characterization of the flow conditions independent of cavitator size, facilitating the examination of the blockage effect, although F_L can be expressed in terms of C_{Qs} and B, i.e. $(4/\pi)C_{Qs}B^2$.

Based on the framework above, figure 10 provides a summary of the distribution of different closure modes corresponding to F_L at two selected Re numbers for four blockage ratios in our experiments. The stable states of the supercavity (i.e. FC, RJ, TV and QV) are primarily considered here for comparison among different blockage ratios. The unstable closure modes shown in the figure refer to PTV for $B = 5\,\%$ and IV for $B = 9\,\%$. The hybrid closure modes (i.e. QVRJ, TVRJ and TVQV) occur over a narrow range of F_L and are thus excluded from the figure.

As figures 10(*a*,*b*) show, at $Re = 6.42 \times 10^5$, a larger F_L is required to reach to a supercavity state from FC as B increases. This trend may be more related to the effect

https://doi.org/10.1017/jfm.2015.680 Published online by Cambridge University Press

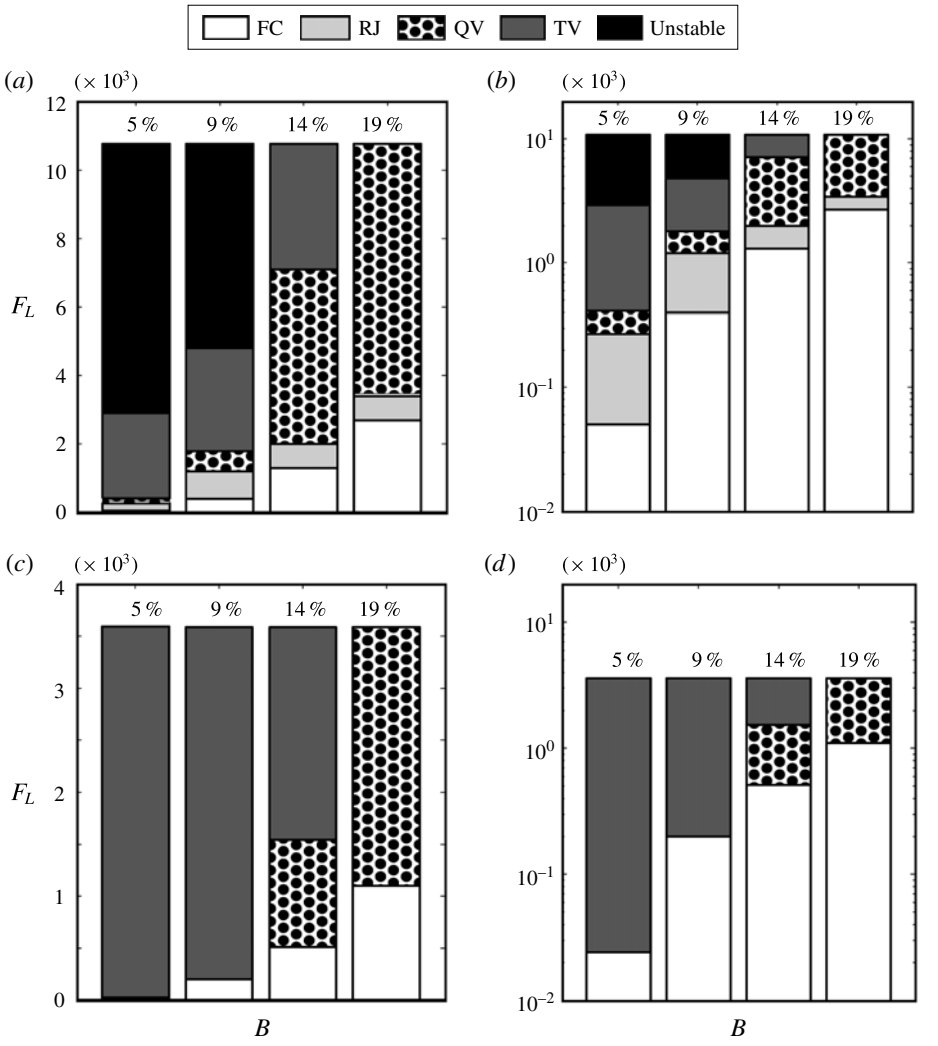


FIGURE 10. Variation of different closure modes with B and F_L at (*a*) $Re = 6.42 \times 10^5$, linear scale (*b*) $Re = 6.42 \times 10^5$, logarithmic scale (*c*) $Re = 1.93 \times 10^6$, linear scale (*d*) $Re = 1.93 \times 10^6$, logarithmic scale. The figures in percentage above the bars represent the values of B.

of cavitator size rather than the blockage ratio. A possible explanation for this trend is that the transition of FC into a supercavity is driven by bubble coalescence. With increasing ventilation flow rate, it is observed that both the size and number of bubbles increase at the periphery of the cavity. For a larger cavitator size, the bubbles in the foam are more sparsely situated and thus more air is required to drive this coalescence process for its transition to a supercavity. Furthermore, as the figures show, for all blockage ratios, the RJ mode is always located between the FC and vortex-based closures and over a narrow range of small F_L consistent with Cox & Clayden (1956). With increasing F_L, the closure transitions gradually from RJ to QV mode, then to TV and unstable modes (i.e. PTV for $B = 5\,\%$, IV for $B = 9\,\%$). It is clear that the range of F_L for QV increases significantly as B increases. Since the extent of the RJ mode

https://doi.org/10.1017/jfm.2015.680 Published online by Cambridge University Press

does not vary appreciably with the change in B, the expansion of the F_L range for QV indicates the tendency to form vortex-based closures as B increases. Note that the range of F_L for QV at $B = 19\,\%$ may persist beyond the upper limit of F_L, as displayed in the figures, which is constrained by the test-section length for observation (since the cavity elongates beyond the test section as F_L increases) in our experimental facility. The above observation regarding blockage effect is supported by a number of prior studies in ventilated supercavitation (e.g. Karlikov & Sholomovich 1966; Zhou *et al.* 2010; Skidmore 2013). For example, the experimental results of Skidmore show that a large water tunnel (i.e. 1.219 m in diameter) leads to RJ closure whereas a smaller one, of 0.305 m diameter, yields only a TV mode. Using a numerical approach and taking into account the effect of blockage on the pressure outside the supercavity, another study by Zhou *et al.* (2010) presented a good match with the Campbell & Hilborne criterion (Campbell & Hilborne 1958) for transition to TV.

As shown in figure 10(*c*,*d*), when Re increases by a factor of three (i.e. $Re = 1.93 \times 10^6$) in comparison with the results in figure 10(*a*,*b*), the trend of the closure mode distribution under the influence of F_L and B changes, although the trend of FC largely remains the same as before. The RJ mode almost disappears for all blockage ratios. Further, the QV mode disappears for the lower values of B of 5 % and 9 %, suggesting that an increase in Re promotes the occurrence of TV mode over QV.

To summarize, based on the presented observations in §§ 3.1, 3.2, it can be concluded that the supercavity closure is not merely a function of Fr, C_{Qs} and σ_C, as discussed by numerous prior studies. Instead, a clear understanding of the physical mechanism is needed while formulating a criterion that determines supercavity closure *viz.* flow conditions, blockage effect and the type of experimental facility, etc. In the following sections, we present a hypothesis for the physical mechanism determining supercavity closure, provide supporting evidence for this hypothesis and use it further to explain experimental observations at SAFL and other facilities.

4. Hypothesis and explanation of observations

A hypothesis regarding the physical mechanism that determines the closure modes of a ventilated supercavity is proposed in order to explain the experimental observations. The hypothesis posits that the closure mechanism is mainly determined by the pressure difference across the gas–water interface at the cavity closure. This pressure difference is constructed in a dimensionless form as $\Delta\tilde{P} = (P_{out} - P_{in})/q = \tilde{P}_{out} - \tilde{P}_{in}$, where $q\,(= 1/2\rho U^2)$ is the dynamic pressure of water in the test section and $\tilde{P}_{in}$ and $\tilde{P}_{out}$ are the dimensionless static pressures inside and just outside the cavity at the closure, respectively (illustrated in figure 11). Note that P_{in} may deviate from the mean cavity pressure due to the internal flows of the supercavity (Pan *et al.* 2010). We hypothesize that the change of Fr, C_{Qs}, B or type of experimental facility leads to the change of $\Delta\tilde{P}$, resulting in the variation of closure modes. Based on a momentum analysis of the control volume at the closure (CV-1 in figure 11), $\Delta\tilde{P}$ is determined by the gas/water phase momentum across the closure, and other physical factors such as surface tension. Among these factors, the net water momentum flux at the closure is dominant since the water density is much higher than that of the ventilated air. It is noteworthy that a number of prior studies have examined cavity closure using physics-based analysis. For instance, Tulin (1964) used momentum theory to show a pressure recovery at the closure of the supercavitating propellers, although his study did not involve different closure modes. Using boundary-layer

https://doi.org/10.1017/jfm.2015.680 Published online by Cambridge University Press

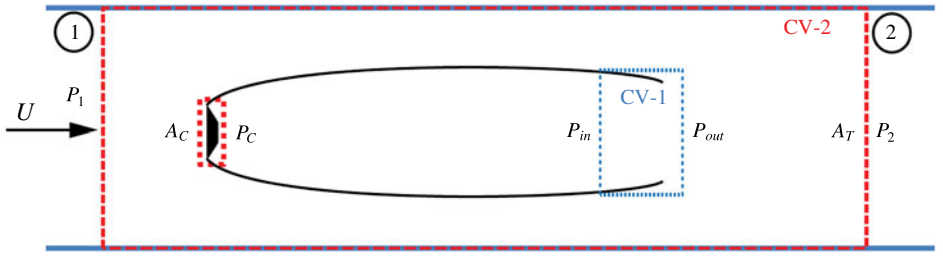


FIGURE 11. (Colour online) Schematic showing the two control volumes related to the supercavity. CV-1 is the control volume at the closure, and CV-2 is the one encompassing the entire cavity.

analysis, Spurk & König (2002) noted that the cavity closure is determined by the change of streamline curvature at the rear portion of the cavity.

According to the conceptual framework above, for the RJ mode, the $\Delta\tilde{P}$ is dominated by the momentum of the re-entrant water jet, while for a vortex-based closure (e.g. TV and QV modes), such pressure difference is significantly smaller in the absence of a re-entrant jet, i.e. $\Delta\tilde{P}_{RJ} \gg \Delta\tilde{P}_{TV}, \Delta\tilde{P}_{QV}$. Nevertheless, the distinct geometric differences between various vortex-based closures suggest that surface tension may contribute to a small variation of pressure difference at the closure which causes the change of closure mode. The influence of surface tension on twin-vortex closures has been admitted in the prior studies by Cox & Clayden (1956), Epshtein (1973), Logvinovich (1973) and more recently by Shi, Itoh & Takami (2000). In the case of a stable air bubble in water, the surface tension on the curved interface induces a pressure difference across a bubble film. In a similar manner, we speculate here that the variation of mean curvature at the closure among different vortex-based closure modes indicates a surface tension effect and a small variation of $\Delta\tilde{P}$. Since a QV closure results from the further splitting of each vortex of a TV closure, it is further hypothesized that the mean curvature at QV closure is smaller than that for a TV mode. Consequently, the pressure difference for the QV mode is smaller than that for TV, i.e. $\Delta\tilde{P}_{QV} > \Delta\tilde{P}_{TV}$. Summarily, the above discussion leads to a $\Delta\tilde{P}$ criterion for the occurrence of different closure modes, i.e. $\Delta\tilde{P}_{RJ} \gg \Delta\tilde{P}_{QV} > \Delta\tilde{P}_{TV}$. Specifically, this criterion implies that RJ mode occurs when $\tilde{P}_{out}$ is significantly higher than $\tilde{P}_{in}$. As $\Delta\tilde{P}$ reduces to a critical value, when it is no longer sufficient to sustain a re-entrant jet, the closure region transitions from RJ to vortex-based closures, and from QV to TV gradually as $\Delta\tilde{P}$ continues to decrease.

The above framework can be further extended to include the blockage effect of a closed-wall water tunnel. This extension is conducted through a momentum analysis on the control volume encompassing the entire supercavity (i.e., CV-2 as shown in figure 11). The CV-2 consists of the horizontal control surfaces coinciding with the test-section walls, vertical surfaces located far upstream (with pressure P_1) and downstream (with pressure P_2) of the cavity and the surfaces that just enclose the cavitator. Assuming that the viscous shear stress on the horizontal control surfaces is negligible, the horizontal momentum equation of CV-2 can be expressed as follows:

$$P_1 A_T = P_2 A_T + F_D, \tag{4.1}$$

where A_T represents the cross-sectional area of the tunnel and F_D is the drag force on the cavitator. To show the connection among the above equation, σ_C and B, the

https://doi.org/10.1017/jfm.2015.680 Published online by Cambridge University Press

Fr	σ_C	$\Delta\tilde{P}$	Cavity states
6.8	0.363	0.354	FC
9.0	0.288	0.279	RJ
15.0	0.221	0.213	QV
20.0	0.210	0.202	TV

TABLE 3. Variation of estimated $\Delta\tilde{P}$ with cavity states for $B = 9\,\%$. Typical dimensional values of pressures inside and outside of the cavity can be obtained from the supplemental files.

following relations are used:

$$F_D = C_D A_C \left(1/2\rho U^2\right) = C_D A_C q \tag{4.2}$$

$$\sigma_C = (P_1 - P_C)/q \tag{4.3}$$

$$A_C/A_T = B^2, \tag{4.4}$$

$$C_D = C_{xD}(1 + \sigma_C) \tag{4.5}$$

where, A_C is the cross-sectional area of disk cavitator and P_C is the internal cavity pressure measured close to the cavitator, as shown in figure 11. C_{xD} is a constant equalling 0.82 for a disk cavitator (Stinebring *et al.* 2001). As a result,

$$(P_2 - P_c)/q = \sigma_C(1 - C_{xD}B^2) - C_{xD}B^2. \tag{4.6}$$

Since a ventilated supercavity is predominantly filled with air, and the air density is significantly smaller than that of water, the difference between P_C and P_{in} cannot be significant. According to Nesteruk (2014), a constant σ_C over the entire cavity surface can be assumed for a ventilated cavity i.e. $P_C \approx P_{in}$. Further, assuming $P_{out} \approx P_2$, we obtain:

$$\Delta\tilde{P} = \sigma_C(1 - C_{xD}B^2) - C_{xD}B^2. \tag{4.7}$$

The above equation shows the direct connection between $\Delta\tilde{P}$ and the blockage ratio. In addition, based on this equation, an estimate of $\Delta\tilde{P}$ can be obtained from the current measurements, which provides experimental evidence of the proposed $\Delta\tilde{P}$ criterion. As an example, table 3 presents estimated $\Delta\tilde{P}$ along with the observed closure modes for $B = 9\,\%$. The different Fr numbers are selected at $C_{Qs} = 0.04$ to include different cavity states in the flow map shown in figure 5. As the table shows, as estimated $\Delta\tilde{P}$ reduces, supercavity transitions from a RJ to a QV, and then to a TV closure, consistent with the proposed criterion. Note that the estimated $\Delta\tilde{P}$ may differ slightly from the $\Delta\tilde{P}$ in the proposed criterion due to the assumptions made to derive (4.7).

Furthermore, we also conducted some experiments to study the effect of a relative change in pressure inside and outside of the cavity on supercavity closure for hybrid modes. In these experiments, the test-section pressure was adjusted independently with fixed Fr and C_{Qs}. The results show that a slight change in the test-section pressure can lead to the transition of hybrid closure modes to stable modes. For instance, it is observed that for QVRJ closure, an increase in test-section pressure (i.e. larger $\tilde{P}_{out}$

https://doi.org/10.1017/jfm.2015.680 Published online by Cambridge University Press

and $\Delta\tilde{P}$) leads to a transition to the RJ mode, whereas a decrease in the pressure (i.e. smaller $\tilde{P}_{out}$ and $\Delta\tilde{P}$) makes the closure transition to a QV mode. It should be noted here that a change in test-section pressure is also coupled with a change in the value of C_Q, which might also contribute to such closure transitions. Similarly, the recent study by Karn *et al.* (2015*b*) suggests an effect of variation in $\Delta\tilde{P}$ on supercavity closure under unsteady flow conditions.

It is worth pointing out that it is difficult to carry out pressure measurements inside and outside of the closure because of the presence of the highly unsteady two-phase flow at the supercavity rear portion, and limitations of the available experimental techniques. However, the evidence presented above provide both qualitative and quantitative support for our proposed $\Delta\tilde{P}$ criterion in determining supercavity closure. The developed framework is now employed to further explain the experimental observations as follows.

4.1. *Variation of closure with Fr or C_{Qs}*

Based on the above discussion, we postulate that the variation of flow conditions (i.e. the change in C_{Qs} and Fr) leads to a change in $\Delta\tilde{P}$, thus causing the transition among closure modes reported in § 3.1. Specifically, for a fixed B and Fr, an increase in C_{Qs} implies an increase in cavity pressure, which results in higher $\tilde{P}_{in}$. Since $\tilde{P}_{out}$ is little dependent on C_{Qs}, the $\Delta\tilde{P}$ is likely to continue decreasing with increasing C_{Qs}. According to the proposed $\Delta\tilde{P}$ criterion, this reduction of $\Delta\tilde{P}$ can lead to a gradual transition of closure modes from RJ to QV, and then to TV, consistent with the observations presented in figure 6. On the other hand, for fixed B and C_{Qs}, an increase in Fr, corresponding to higher water velocity, leads to an increment in fluid dynamic pressure and a decrement in static pressure outside the closure, and thus reduces $\tilde{P}_{out}$. However, the increase in Fr also leads to a reduction in $\tilde{P}_{in}$ due to the change in cavity geometry. Therefore, its net effect on $\Delta\tilde{P}$ cannot be readily decoupled from C_{Qs}. This phenomenon causes some subtle variation in closure-mode transition at different C_{Qs} values upon change in Fr, as observed in figures 5 and 7.

4.2. *Variation of supercavity closure with blockage ratios*

The equation (4.7) provides a direct link between $\Delta\tilde{P}$ and blockage ratios. As it shows, higher blockage leads to smaller $\Delta\tilde{P}$, promoting the occurrence of TV modes according to the proposed $\Delta\tilde{P}$ criterion. This conclusion is consistent with the experimental observations and prior studies reported in § 3.2. It worthwhile noting that at a high blockage, two additional effects have a bearing on the $\Delta\tilde{P}$. First, the growth of the turbulent boundary layer at the test-section walls effectively reduces the flow area and leads to a longitudinal pressure gradient in the test section (Wu, Whitney & Brennen 1971). Second, the wall viscous effect, which is neglected in the derivation of (4.7), may also become substantial. Nevertheless, these effects would contribute to a greater drop in $\tilde{P}_{out}$, as compared to $\tilde{P}_{in}$, thus resulting in a lower $\Delta\tilde{P}$, which is in favour of the occurrence of TV mode.

As shown in figure 10, the TV mode is dominant, even at the lowest blockage ratio, which indicates the presence of a considerable blockage effect in our experiments according to the proposed framework. This assessment is supported by a recent experiment using a large water tunnel (Skidmore 2013). In this study, a maximum blockage ratio of 1.6 % is observed to yield RJ closure as the dominant mode,

https://doi.org/10.1017/jfm.2015.680 Published online by Cambridge University Press

which is still significantly lower than the smallest B in our experiments (i.e. 5 %). It is important to note that the effect of cavitator size may also play a role when interpreting the observations of RJ closure modes at different blockage ratios. According to a number of prior studies (Gopalan & Katz 2000; Callenaere *et al.* 2001; Kshatriya *et al.* 2007), a slender cavity generated from a small cavitator does not yield sufficient adverse pressure gradient to create a re-entrant jet and consequently, TV is favoured. Gadd & Grant (1965) conjectured that the observation of RJ modes in their water tunnel experiments with relatively high blockage (i.e., $B = 7$–11 %) may be related to the large size of cavitators used (i.e., 8–14 cm in diameter). Therefore, it is possible that the attainment of the RJ closure mode in a closed-wall facility requires not only a low B, but also a cavitator of sufficient size.

5. Summary and discussion

A study has been conducted to investigate the physical mechanisms determining the closure formation and transition between different closure modes for ventilated supercavitation. We carried out the experiments in a closed-wall recirculating water tunnel to image ventilated supercavity closure using high speed and high-resolution photography and to measure pressure inside the cavity over a wide range of flow conditions. Apart from the classical closure modes reported in the literature, the study has revealed a number of new closure modes occurring during the transition between classical modes, or under very specific flow conditions. We construct closure maps to depict the flow regimes of each closure mode as a function of Fr and C_{Qs} for different blockage ratios. Based on the closure map, a critical ventilation flow rate is identified at each blockage ratio, and the corresponding critical air entrainment coefficient is found to be independent of blockage ratio. It has also been observed that in the process of generating a supercavity by increasing ventilation flow rate, the cavitation number gradually reduces to a minimum value and stays fixed upon further increment in ventilation rate. Once a supercavity is formed, the ventilation rate can be decreased to a much lower value with no change in cavitation number while still maintaining a supercavity. This process is accompanied by a transition in closure modes, which generally goes from twin vortex, to quad vortex and then to re-entrant jet. In addition, the blockage effect is shown to play an important role in promoting the occurrence of twin-vortex closure modes. Subsequently, a physical framework governing the variation of closure modes is proposed, and is used to explain mode transition upon change of flow conditions, including the blockage effect. In the discussion below, this framework is further extended to examine the closure variation across different types of flow facilities, the natural supercavity closure and the pulsating supercavity reported in the literature, and sheds light on a recent numerical study of supercavity internal flows.

5.1. *Closure of a ventilated supercavity in a free-surface facility*

The fundamentals established in § 4 can be extended to explain the different observations of supercavity closure obtained in a free-surface facility. For such a facility, P_{out} is primarily controlled by the pressure at the free surface and the depth of submergence, which determines the hydrostatic pressure outside the supercavity, whereas P_{in} is largely regulated by the ventilation flow rate. Specifically, unlike the closed-wall tunnel, both the pressure upstream of the cavity and the pressure outside the closure in a free-surface facility are dictated by the presence of the free surface, and are less dependent on Fr. Thus, for the same set of Fr, C_{Qs} and upstream

https://doi.org/10.1017/jfm.2015.680 Published online by Cambridge University Press

cavity pressure, the pressure difference at the closure ($\Delta\tilde{P}$) in a free-surface facility is generally larger than that in a closed-wall tunnel. According to our discussion in § 4, this difference in attainable $\Delta\tilde{P}$ between facilities implies that free-surface facilities favour the occurrence of RJ over TV compared with the closed-wall tunnels influenced by the blockage effect. Similarly, the above discussion also suggests that for the same Fr and C_{Qs}, an increasing depth of submergence leads to a consequent decrease in C_Q, and promotes RJ over TV closure in a free-surface facility. These inferences are consistent with general trends of the closures observed in closed wall and free-surface facilities (e.g. Cox & Clayden 1956; Campbell & Hilborne 1958; Epshtein 1973). Note that our reasoning does not preclude the possibility of TV occurrence in a free-surface facility, or the formation of RJ in a closed wall tunnel, but rather provides a qualitative comparison of the trends of occurrence of RJ or TV modes in different types of facilities.

5.2. *On the closure of a natural supercavity*

In a natural supercavity, the P_{in} is equal to the vapour pressure. Therefore P_{out}, determined by B in a closed-wall tunnel or hydrostatic pressure head at the cavity closure for a free-surface facility, is usually much higher than P_{in}. This large difference in pressure leads to a high value of $\Delta\tilde{P}$, and the occurrence of RJ closure is favoured based on our discussion in § 4. To verify this, natural supercavitation experiments are conducted at SAFL by systematically varying Fr at different values of B, and it is observed that the RJ closure is the dominant mode for a natural supercavity (figure 12). As the figure shows, the RJ closure is marked by the presence of such recurrent toroidal vortices in the wake of the cavity. According to Semenenko (2001*a*), the re-entrant jet at the cavity rear creates a foamy region, which moves as a toroidal vortex, experiencing tangential stresses from the cavity wall and the forces due to the pressure gradient in the central part of the cavity. The growth of these vortices continues with the incoming vapour–water mixture until a time when both these forces (i.e. tangential force and pressure force) are equal and the vortices are ejected in a recurrent fashion. This invariable occurrence of RJ closure for natural supercavitation agrees with the experiments reported from different facilities (e.g. Logvinovich 1973; Hrubes 2001; Semenenko 2001*a*; Vlasenko 2003; Zhang *et al.* 2007; Ahn *et al.* 2013).

5.3. *On the occurrence of pulsating cavity closure*

Based on our discussion in § 4, we posit that cavity pulsation may result from the periodic pressure fluctuations inside the cavity, which necessitates the presence of a free surface in the facility since the tunnel walls would restrict the radial expansion of the cavity associated with pulsation. Despite the debate regarding the mechanism of PC in the literature, a careful scrutiny of the experimental facilities in all the reported studies reveals the presence of a free surface either in the test section, or in a tank connected to the test section (e.g. Song 1961; Michel 1984; Skidmore 2013). This remark is further supported through a comparison among (Silberman & Song 1961; Skidmore 2013) and our current study. Specifically, Silberman & Song observed PC across a much wider range of flow conditions in a vertical water tunnel with two free surfaces compared to Skidmore's experiments in a free-surface flume. In addition, in our current experiments at the SAFL closed-wall water tunnel, the pulsating cavity is not obtained even though the experiments are conducted over a wide range of water velocity and air ventilation flow rate at all blockage ratios.

https://doi.org/10.1017/jfm.2015.680 Published online by Cambridge University Press

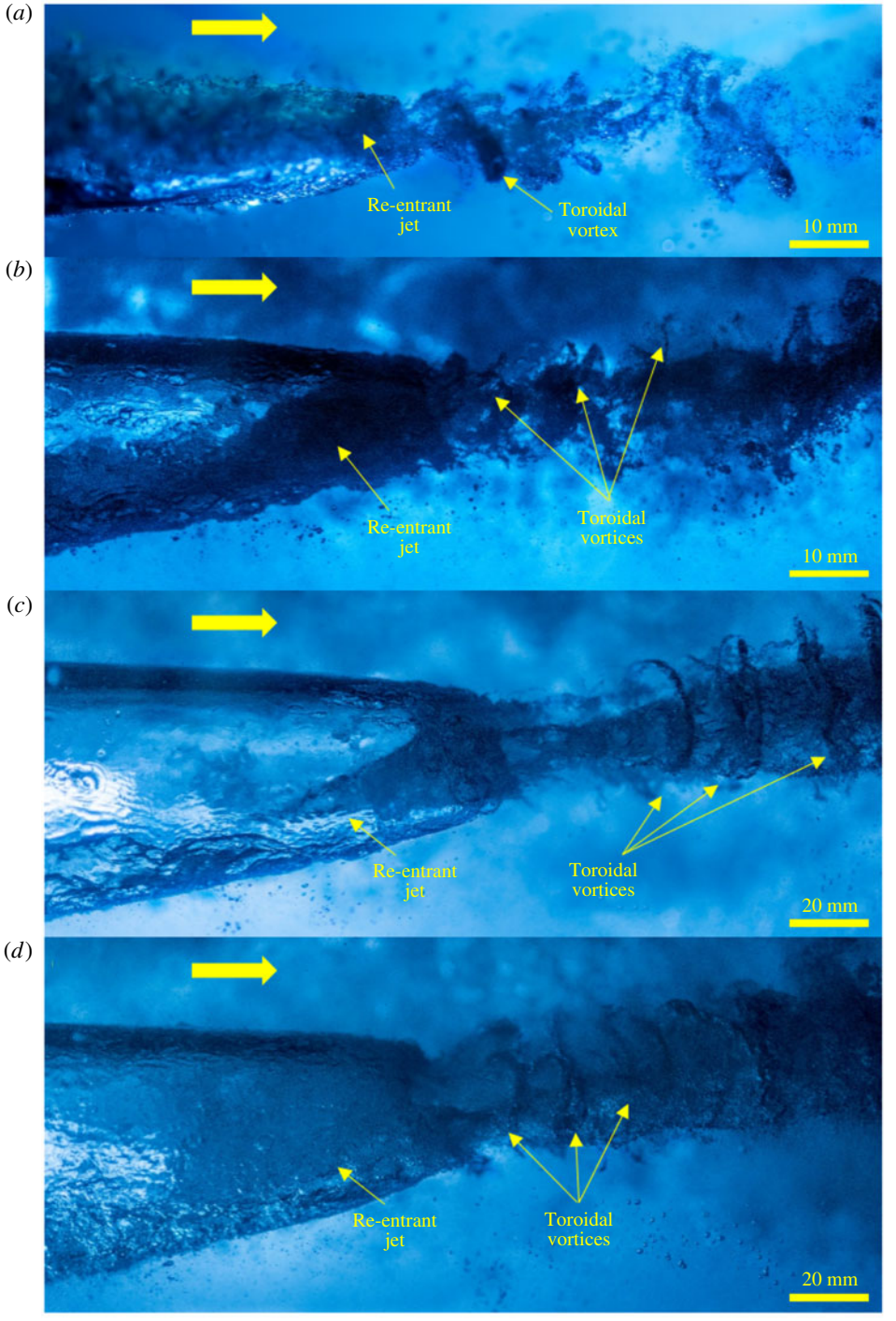


FIGURE 12. (Colour online) Closure images of natural supercavity at (*a*) $B = 5\,\%$, (*b*) $B = 9\,\%$, (*c*) $B = 14\,\%$, (*d*) $B = 19\,\%$. Note that the vortices are filled with water vapour. The horizontal arrow indicates the direction of the water flow.

https://doi.org/10.1017/jfm.2015.680 Published online by Cambridge University Press

5.4. *Dependence of supercavity behaviour upon internal cavity flow*

The previous sections have delineated how our proposed hypothesis can be used to explain the supercavity closure under a variety of flow environments. It is noteworthy that one of the key premises of our theory is that the internal flow within a ventilated supercavity can yield a non-uniform pressure distribution, and thus affect cavity closure. However, due to the experimental challenges involved in quantifying flows across a gas–water interface, very few researchers have examined internal cavity flows. Using a numerical approach, a recent study by Kinzel, Lindau & Kunz (2009) shows that the internal flow within the cavity core is intricately related to the ventilation flow rate. For C_{Qs} greater than a threshold value (i.e., $C_{Qs,thres}$), the mean flow velocity inside the cavity core (U_C) is in the downstream direction (i.e., $U_C > 0$) and a pressure-driven twin-vortex cavity results. For C_Q close to $C_{Qs,thres}$, there is negligible flow of air inside the cavity core and the mean flow velocity is close to zero, and a RJ closure occurs. On the other hand, when C_{Qs} is less than $C_{Qs,thres,}$ there is flow recirculation inside the cavity and the mean flow velocity inside the cavity core is in the upstream direction (i.e., $U_C < 0$). Here, we combine their numerical results with our proposed framework in § 4 to explain some interesting observations pertaining to closure transitions in our experiments, which highlights the significance of internal flow within a cavity. In particular, we will focus on the following four observations as noted in § 3:

(1) *Critical ventilation flow rate*: our experiments show a critical ventilation flow rate (Q_{crit}) for each blockage ratio, below which the supercavity collapses (i.e. transition to FC) as Fr is decreased from a large initial value. As shown in table 3, large $\Delta\tilde{P}$ values lead to a transition of a supercavity into FC state. Based on our framework in § 4.1, as Fr is decreased at a fixed B (or, cavitator cross-sectional area A_c), the consequent reduction in dynamic pressure and increment of test-section pressure leads to an increment in $\tilde{P}_{out}$. For the cavity to be sustained, $\tilde{P}_{in}$ has to be high enough to ensure $U_C > 0$, and prevent water at the cavity rear rushing into the upstream portion of the cavity causing cavity collapse. Since $\tilde{P}_{in}$ at different Fr depends upon the ventilation flow rate, there exists a critical ventilation flow rate corresponding to each cavitator, such that $\Delta\tilde{P}$ is small enough to prevent cavity collapse in the range of Fr tested. This argument has been supported by examining the dependence of Q_{crit} on cavitator size presented in figure 13, which shows direct proportionality of Q_{crit} with respect to A_c.

(2) *Ventilation hysteresis*: significantly higher ventilation flow rate is required to establish a supercavity than to sustain it. FC consists of a number of closely packed small individual bubbles, which increase both in number and size upon increments in ventilation flow rate due to bubble coalescence events (Wu 1972; Kshatriya *et al.* 2007). With further increase in the ventilation flow rate, the bubbles along the periphery are subjected to high-shear flow, resulting in elongation and coalescence until a clear supercavity is formed. Thus, to drive this coalescence process into a supercavity necessitates sufficient ventilation flow to generate a pressure-driven twin-vortex cavity with $U_C > 0$. However, once a supercavity is formed, it is possible to maintain the cavity by lowering C_{Qs}. Upon such reduction in ventilation flow, the internal cavity flow adapts itself (i.e., U_C reduces and becomes non-positive) with a simultaneous change in closure mechanism.

(3) *Path selectivity*: RJ closure cannot be generated from a foamy cavity by increasing ventilation flow rate. It can only be obtained by gradually decreasing ventilation flow rate from an established TV closure. This phenomenon is related

https://doi.org/10.1017/jfm.2015.680 Published online by Cambridge University Press

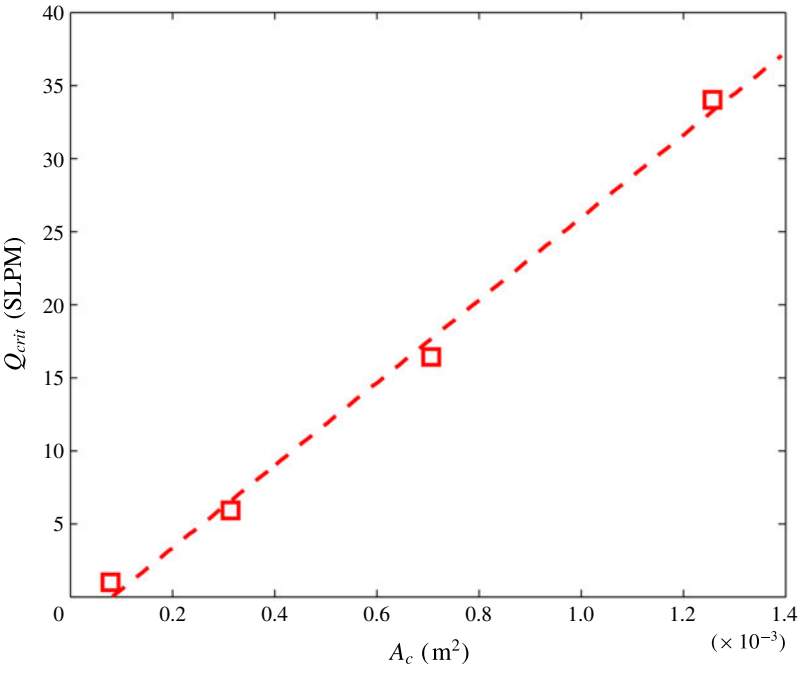


FIGURE 13. (Colour online) Dependence of Q_{crit} upon A_c. The square symbol denotes the Q_{crit} corresponding to each cavitator used in the experiments, and the straight line is the least-square linear fit of the square symbols.

to the ventilation hysteresis discussed above. According to our discussion, a minimum ventilation flow rate (i.e. $C_{Qs,thres}$) is required to drive the process of bubble coalescence for generating the supercavity. For RJ closure, U_C is close to zero, which generally corresponds to a large $\Delta\tilde{P}$ and air entrainment coefficient below $C_{Qs,thres}$. Therefore, RJ closure can only be obtained by lowering C_{Qs} after the supercavity is formed.

(4) *Susceptibility*: the formation of RJ closure is sensitive to the changes in Fr and C_{Qs}. During the transition from TV to RJ closure, an abrupt reduction in Fr or C_{Qs} leads to cavity collapse. Further, RJ closure is stable only in a very narrow range of Fr and C_{Qs}. As discussed above, the attainment of RJ requires U_C to reduce to a value very close to zero. During this process, an abrupt change in water velocity or ventilation rate (corresponding to a change in Fr or C_{Qs}) could set up a strong recirculation in the upstream direction (i.e. $U_C < 0$), causing cavity breakdown.

However, to substantiate above reasoning and elucidate the flow physics inside a supercavity requires some advanced imaging experiments across the water–supercavity interface, which might be considered in future investigations.

Acknowledgement

This work is supported by Office of Naval Research – United States (Program manager: Dr R. Joslin) under grant no. N000140910141 and the startup of J.H. from the University of Minnesota. A.K. acknowledges support from the Doctoral Dissertation Fellowship, Graduate School, University of Minnesota Twin cities.

https://doi.org/10.1017/jfm.2015.680 Published online by Cambridge University Press

We also acknowledge the help of an undergraduate student from Department of Aerospace Engineering and Mechanics, Mr R. De, who helped with digital photography.

Supplementary data

Supplementary data is available at http://dx.doi.org/10.1017/jfm.2015.680.

REFERENCES

AHN, B. K., KIM, J., JUN, Y., KIM, H. & LEE, C. 2013 Experimental and numerical study of natural supercavitating flows. In *Proceedings of the PRADS2013, CECO, Changwon City, Korea*.

BUYVOL, V. N. 1980 *Slender Cavities in Flows With Perturbations*, Nauvoka Dunka; (in Russian).

CALLENAERE, M., FRANC, J., MICHEL, J. & RIONDET, M. 2001 The cavitation instability induced by the development of a re-entrant jet. *J. Fluid Mech.* **444**, 223–256.

COX, R. & CLAYDEN, W. 1956 Air entrainment at the rear of a steady cavity. In *Proceedings of the Symposium on Cavitation in Hydrodynamics, London*.

EPSHTEIN, L. 1973 Characteristics of ventilated cavities and some scale effects. In *Proceedings of the International Symposium IUTAM, Unsteady Water Flow with High Velocities*, pp. 173–185. Nauka.

GADD, G. & GRANT, S. 1965 Some experiments on cavities behind disks. *J. Fluid Mech.* **23** (4), 645–656.

GOPALAN, S. & KATZ, J. 2000 Flow structure and modeling issues in the closure region of attached cavitation. *Phys. Fluids* **12** (4), 895–911.

CAMPBELL, I. J. & HILBORNE, D.V. 1958 Air entrainment behind artificially inflated cavity. In *Proceedings of the Second Symposium on Naval Hydrodynamics, Washington*.

HRUBES, J. 2001 High-speed imaging of supercavitating underwater projectiles. *Exp. Fluids* **30** (1), 57–64.

KAPANKIN, Y. N. & GUSEV, A. V. 1984 Experimental research of joint influence of fluid and lift power of cavitator on character of flow in cavity rear part and gas departure from it. *Proc. CAHI* **2244**, 19–28.

KARLIKOV, V., REZNICHENKO, N., KHOMYAKOV, A. & SHOLOMOVICH, G. 1987 A possible mechanism for the emergence of auto-oscillations in developed artificial cavitation flows and immersed gas jets. *Fluid Dyn.* **22** (3), 392–398.

KARLIKOV, V. & SHOLOMOVICH, G. 1966 Method of approximate account for the wall effect in cavitation flow around bodies in water tunnels. *Fluid Dyn.* **1** (4), 61–64.

KARN, A., ARNDT, R. E. A. & HONG, J. 2015*a* Dependence of Supercavity closure upon flow unsteadiness. *Exp. Therm. Fluid Sci.* **68**, 493–498.

KARN, A., MONSON, G., ELLIS, C., HONG, J., ARNDT, R. & GULLIVER, J. 2015*b* Mass transfer studies across ventilated hydrofoils: A step towards hydroturbine aeration. *Intl J. Heat Mass Transfer* **87**, 512–520.

KINZEL, M. P., LINDAU, J. W. & KUNZ, R. F. 2009 Air entrainment mechanisms from artificial supercavities: insight based on numerical simulations. In *Proceedings of the 7th International Symposium on Cavitation, CAV 2009, Ann Arbor*, vol. 136.

KAWAKAMI, E. 2010 Investigation of the behavior of ventilated supercavities, *MS Thesis*, University of Minnesota, Twin cities.

KAWAKAMI, E. & ARNDT, R. E. A. 2011 Investigation of the behavior of ventilated supercavities. *J. Fluid Engng* **133** (9), 091305,1–11.

KSHATRIYA, S., PATWARDHAN, A. & EAGLESHAM, A. 2007 Experimental studies of ventilated cavities in a channel. *Chem. Engng Sci.* **62** (4), 979–989.

KUKLINSKI, R., CASTANO, J. & HENOCH, C. 2001 Experimental study of ventilated cavities on dynamic test model. In *CAV 2001: Fourth International Symposium on Cavitation. Naval Undersa Weapons Center, Newport, RI*.

LOGVINOVICH, G. V. 1973 *Hydrodynamics of Free-Boundary Flows*. Halsted Press.

https://doi.org/10.1017/jfm.2015.680 Published online by Cambridge University Press

MICHEL, J. 1984 Some features of water flows with ventilated cavities. *Trans. ASME J. Fluids Engng* **106** (3), 319–326.

NESTERUK, I. 2014 Shape of slender axisymmetric ventilated supercavities. *J. Comput. Engng* **2014**, 501590,1–18.

PARYSHEV, E. 2003 Mathematical modelling of unsteady cavity flows. In *Proceedings of Fifth International Symposium on Cavitation (CAV 2003), Osaka, Japan*, pp. 1–18.

PENG, X., WANG, Z., PAN, S. & YAN, K. 2006 Generation mechanism of ventilated supercavitation in an axisymmetric body with cavitator. In *Proceedings of Sixth International Symposium on Cavitation, CAV2006, Wageningen, Netherlands*.

PAN, Z., LU, C., CHEN, Y. & HU, S. 2010 Numerical study of periodically forced-pitching of a supercavitating vehicle. In *Proceedings of Ninth International Conference on Hydrodynamics, Shanghai, China*.

SAVCHENKO, Y. 2001 Supercavitation-problems and perspectives. In *Fourth International Symposium on Cavitation. California Institute of Technology Pasadena, California*, vol. 200.

SEMENENKO, V. N. 2001*a* *Artificial Supercavitation: Physics and Calculation*. Ukrainian Academy of Sciences, Kiev Inst of Hydromechanics.

SEMENENKO, V. N. 2001*b* *Dynamic Processes of Supercavitation and Computer Simulation*. Ukrainian Academy of Sciences, Kiev Inst of Gydromechanics.

SHI, H., ITOH, M. & TAKAMI, T. 2000 Optical observation of the supercavitation induced by high-speed water entry. *Trans. ASME J. Fluids Engng* **122** (4), 806–810.

SILBERMAN, E. & SONG, C. S. 1961 Instability of ventilated cavities. *J. Ship. Res.* **5** (1), 13–33.

SKIDMORE, G. 2013 The pulsation of ventilated supercavities, *Master of Science thesis*, Department of Aerospace Engineering, Pennsylvania State University.

SKIDMORE, G., BRUNGART, T. A., LINDAU, J. W. & MOENY, M. J. 2015 Noise generated by ventilated supercavities. *Noise Control Engr. J.* **63** (1), 94–101.

SONG, C. S. 1961 Pulsation of ventilated cavities. (No. 32 B). Saint Anthony Falls Laboratory, University of Minnesota.

SPURK, J. & KÖNIG, B. 2002 On the gas loss from ventilated supercavities. *Acta Mech.* **155**, 125–135.

STINEBRING, D. R., BILLET, M. L., LINDAU, J. W. & KUNZ, R. F. 2001 Developed cavitation-cavity dynamics, DTIC Document.

TULIN, M. P. 1964 Supercavitating propellers, momentum theory. (No. TR-121-4). Hydronautics Inc. Laurel MD: DTIC Document.

VLASENKO, Y. D. 2003 Experimental investigation of supercavitation flow regimes at subsonic and transonic speeds. In *Fifth International Symposium on Cavitation, Osaka, Japan*.

WU, T., WHITNEY, A. K. & BRENNEN, C. 1971 Cavity-flow wall effects and correction rules. *J. Fluid Mech.* **49** (2), 223–256.

WU, T. 1972 Cavity and wake flows. *Annu. Rev. Fluid Mech.* **4**, 243–284.

ZHANG, X., WEI, Y., ZHANG, J., WANG, C. & YU, K. 2007 Experimental research on the shape characters of natural and ventilated supercavitation. *J. Hydrodyn.* B **19** (5), 564–571.

ZHOU, J., YU, K., MIN, J. & YANG, M. 2010 The comparative study of ventilated super cavity shape in water tunnel and infinite flow field. *J. Hydrodyn.* B **22** (5), 689–696.

https://doi.org/10.1017/jfm.2015.680 Published online by Cambridge University Press